# BioOne COMPLETE

# Induction of Chromosomal Aberrations after Exposure to the Auger Electron Emitter Iodine-125, the β–-emitter Tritium and Cesium-137 γ rays

Authors: Unverricht-Yeboah, M., von Ameln, M., and Kriehuber, R.

# Induction of Chromosomal Aberrations after Exposure to the Auger Electron Emitter Iodine-125, the β−-emitter Tritium and Cesium-137 γ rays

M. Unverricht-Yeboah,[1] M. von Ameln, R. Kriehuber

Forschungszentrum Jülich, Department of Safety and Radiation Protection, Jülich, Germany

Unverricht-Yeboah M, von Ameln M, Kriehuber R. Induction of Chromosomal Aberrations after Exposure to the Auger Electron Emitter Iodine-125, the β−-emitter Tritium and Cesium-137 γ rays. Radiat Res. 201, 479–486 (2024).

High-LET-type cell survival curves have been observed in cells that were allowed to incorporate $^{125}$I-UdR into their DNA. Incorporation of tritiated thymidine into the DNA of cells has also been shown to result in an increase in relative biological effectiveness in cell survival experiments, but the increase is smaller than observed after incorporation of $^{125}$I-UdR. These findings are explained in the literature by the overall complexity of the induced DNA damage resulting from energies of the ejected electron(s) during the decay of $^3$H and $^{125}$I. Chromosomal aberrations (CA) are defined as morphological or structural changes of one or more chromosomes, and can be induced by ionizing radiation. Whether the number of CA is associated with the linear energy transfer (LET) of the radiation and/or the actual complexity of the induced DNA double-strand breaks (DSB) remains elusive. In this study, we investigated whether DNA lesions induced at different cell cycle stages and by different radiation types [Auger-electrons ($^{125}$I), β− particles ($^3$H), or γ radiation ($^{137}$Cs)] have an impact on the number of CA induced after induction of the same number of DSB as determined by the γ-H2AX foci assay. Cells were synchronized and pulse-labeled in S phase with low activities of $^{125}$I-UdR or tritiated thymidine. For decay accumulation, cells were cryopreserved either after pulse-labeling in S phase or after progression to $G_2$/M or $G_1$ phase. Experiments with γ irradiation ($^{137}$Cs) were performed with synchronized and cryopreserved cells in S, $G_2$/M or $G_1$ phase. After thawing, a CA assay was performed. All experiments were performed after a similar number of DSB were induced. CA induction after $^{125}$I-UdR was incorporated was 2.9-fold and 1.7-fold greater compared to exposure to γ radiation and radiation from incorporated tritiated thymidine, respectively, when measured in $G_2$/M cells. In addition, measurement of CA in $G_2$/M cells after incorporation of $^{125}$I-UdR was 2.5-fold greater when compared to cells in $G_1$ phase. In contrast, no differences were observed between the three radiation qualities with respect to exposure after cryopreservation in S or $G_1$ phase. The data indicate that the 3D organization of replicated DNA in $G_2$/M cells seems to be more sensitive to induction of more complex DNA lesions compared to the DNA architecture in S or $G_1$ cells. Whether this is due to the DNA organization itself or differences in DNA repair capability remains unclear.  © 2024 by Radiation Research Society

[1] Marcus Unverricht-Yeboah, Forschungszentrum Jülich, Department of Safety and Radiation Protection, Wilhelm-Johnen-Strasse Jülich, Germany; email: m.unverricht@fz-juelich.de.

## INTRODUCTION

The biological effectiveness of ionizing radiation depends not only on dose or dose rate but also on the LET (linear energy transfer) of the radiation. For example, a particle with an LET of 100 keV/μm causes a minimum of 15 ionizations when traversing a single DNA double-helix molecule and, therefore, may induce complex DNA lesions, (1–5) which are repaired less efficiently or completely (6–8) compared to a lower LET radiation, resulting in a higher relative biological effectiveness. When Auger electron emitters (AEE) such as iodine-125 ($^{125}$I) decay, low-energy Auger electrons with a short range of 1–10 nm (9) deposit a high amount of energy in an extremely small volume, which is why Auger electron emission is considered as high-LET radiation (10–12). Iodine-125 emits an average of 13 low-energy Auger electrons per decay (13) and is known to induce complex DNA lesions when incorporated into DNA (14, 15), resulting in high-LET type effects (e.g., cell survival curves with no shoulder region) (16–18).

To investigate whether the complexity of DNA lesions affects the formation of chromosomal aberrations (CA), three different radiation qualities were studied, namely $^{137}$Cs γ rays (662 keV),$^{125}$I incorporated into cellular DNA as $^{125}$I-iododeoxyuridine ($^{125}$I-UdR) and $^3$H, incorporated into cellular DNA as tritiated thymidine. DNA-incorporated tritiated thymidine is known to have a slightly increased RBE compared to low-LET radiation (19) because of the low energy of the β particles emitted during decay (mean energy of 5.7 keV). Energy spectra of $^{125}$I Auger electrons show maximum energies up to 35.4 keV, with most Auger electrons having very low energies of 20–500 eV (9, 20). To classify the biological effectiveness of the two very different radionuclides, we used γ radiation as a reference radiation for comparison.

In addition to the impact of varying complexity of DNA lesions induced by the radiation qualities used here on CA, this study also investigates whether the cell cycle phase in

479

which the exposure occurs has an impact on the induction of CA. Cell cycle phases differ with respect to 3D chromatin structure, which may have an impact on the extent of the complexity of DNA lesions and/or their repair. Whereas chromatin in S phase and in the transcriptionally active $G_1$ phase is relatively relaxed and open, chromatin in $G_2$ phase and mitosis is more condensed and/or already densely packed; this is likely the main reason why $G_2/M$ cells are the most radiosensitive cells (21). Whether DSBs are converted into chromosomal aberrations depends on the fidelity of different principal DNA repair pathways: non-homologous end joining (NHEJ), which is available throughout the cell cycle, and homologous recombination (HR), which is only active in S and $G_2$ phase (22–26).

To compare all radiation qualities and to avoid microdosimetric approaches with rather high dose uncertainties, especially for the low-energy electrons (particularly in the case of Auger electron emitter (AEE) $^{125}I$), the induction of chromosomal aberrations was normalized to induction of γ-H2AX foci, which are widely regarded and accepted as an indicator of DSB (27–30).

## MATERIALS AND METHODS

### Cell Culture and Synchronization

All experiments were carried out in Jurkat cells. Details regarding the origin of the human acute T-cell leukemia Jurkat cells and the standard cell culture conditions have been described previously (31). However, the cells in this study were cultured without penicillin/streptomycin in RPMI 1640 medium (PAA Laboratories, Pasching, Austria) with 10% inactivated fetal bovine serum (Biochrom, Berlin, Germany). The doubling time of Jurkat cells was approximately 24 h. Jurkat cells were synchronized at the $G_1/S$ boundary by aphidicolin (Sigma-Aldrich, Munich, Germany). Cells were incubated for 16 h with aphidicolin at a final concentration of 3 μg/ml, followed by washing the cells twice with standard growth medium, with one washing step including centrifugation of the cells for 5 min at 300 × g at room temperature (RT), removal of the supernatant and careful resuspension of the cells. After removal of aphidicolin, cells were cultured in growth medium for 10 h, and then cells were incubated again with aphidicolin at a final concentration of 3 μg/ml for 16 h. Afterward, the synchronized cells were washed twice and cultured in standard growth medium at a final cell concentration of $1 \times 10^6$ cells/ml. The cell cycle of the cells was monitored after synchronization and during labeling, as described below. Directly after synchronization with aphidicolin, the percentage of cells in $G_1$ phase was approximately 87%. The S phase of Jurkat cells lasts approximately 7 h. The cells are in the $G_2/M$ phase and $G_1$ phase about 7.5 h and 12–14 h after aphidicolin withdrawal, respectively.

### Exposure to $^{125}I$-UdR, Tritiated Thymidine and γ rays in the Cryopreserved State and Thawing

Synchronized cells were pulse-labeled for 1 h with 0.5–1 kBq/ml of $^{125}I$-iododeoxyuridine (carrier-free; specific activity 2,000 Ci/mmol; Hartmann Analytic, Braunschweig, Germany) or 100–500 kBq/ml tritiated thymidine (carrier-free; specific activity 60–90 Ci/mmol; Hartmann Analytic). To maximize the incorporation of $^{125}I$-UdR or tritiated thymidine into the DNA, 0.01 μM/ml fluorodeoxyuridine (FUdR, Fluka, Munich, Germany) and 0.1 μM/ml deoxycytidine (CdR, Fluka) were added to the cell culture medium during labeling. Fluorodeoxyuridine inhibits the cellular synthesis of cytidine and thymidine, thereby increasing the incorporation of the thymidine analogues $^{125}I$-UdR and tritiated thymidine. Deoxycytidine was added to compensate for the inhibition of cytidine synthesis by fluorodeoxyuridine. Control cells
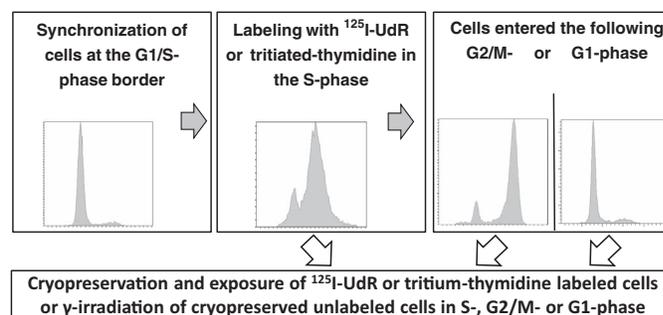


**FIG. 1.** Schematic representation of the exposure conditions visualized by representative flow cytometric histograms after synchronization and the subsequent S, $G_2/M$, or $G_1$ phase. Directly after synchronization, the percentage of cells in $G_1$ phase was approximately 87 ± 3%, and approximately 78 ± 3%, 75 ± 7% and 85 ± 2% entered the subsequent S, $G_2/M$ and $G_1$ cell-cycle phases synchronously, respectively (data based on at least seven independent experiments). After synchronization, cells were labeled in S phase with low activities of $^{125}I$-UdR or tritiated thymidine. For decay accumulation, cells were cryopreserved either after labeling in S phase or after progression to $G_2/M$ or $G_1$ phase. Unlabeled cryopreserved cells were γ-irradiated in S, $G_2/M$ or $G_1$ phase.

were identically treated, except that $^{125}I$-UdR or tritiated thymidine was replaced with non-radioactive I-UdR or thymidine (Fluka), respectively. After labeling, cells were washed once with growth medium and then cultured with standard growth medium in an incubator (Sanyo, Bad Nenndorf, Germany) until cryopreservation of the cells for accumulation of the desired numbers of $^{125}I$ or $^3H$ decays.

For the cryopreservation process, cells were centrifuged (5 min at 300 × g at room temperature), supernatant was removed and cells were resuspended in cryopreservation medium [FBS (Biochrom, Berlin, Germany) plus 10% dimethyl sulfoxide (Carl Roth, Karlsruhe, Germany)], aliquoted in cryogenic vials (VWR International, Darmstadt, Germany) and stored at –150°C for decay accumulation. To achieve a consistent and reproducible freezing profile of –1°C/min, Cell Freezing Vial Containers (Fisher Scientific, Roskilde, Denmark) were used. Before storage, cell numbers were measured (Casy Counter; Schärfe System, Reutlingen, Germany) and aliquots of the cell suspension were taken to determine the activity of incorporated $^{125}I$-UdR or tritiated thymidine. The activity of $^{125}I$ was determined with a gamma-counter (1480 Wizard TM3, Perkin Elmer, Rodgau, Germany). The gamma-counter was calibrated using a $^{125}I$ standard solution, which was previously measured in the whole-body counter of the personal dosimetry unit at Forschungszentrum Jülich. The whole-body counter is regularly calibrated using a commercially purchased calibrated solution (Eckert & Ziegler Nuclitec, Braunschweig, Germany). The tritium activity was determined by a liquid scintillation counter (calibrated with a commercially purchased tritium standard) and measurements performed by the operational analysis laboratory of the Forschungszentrum Jülich. Activity measurements and cell numbers were obtained to calculate cryopreservation time to achieve desired numbers of accumulated decays per cell, as previously described (31). For $^{125}I$-UdR and tritiated thymidine, about 50 and 2,100 decays per cell were accumulated within 18–47 days, respectively. The fraction of iodine-125 or tritium that decays during the labeling procedure until cells are cryopreserved is extremely low, due to the applied low activity concentrations. About 95% of the decays/cell occurred in the cryopreserved state in all experiments.

For the examinations, a fraction of the cells was cryopreserved in S phase after labeling with $^{125}I$-UdR or tritiated thymidine. The other labeled cells progressed into the $G_2/M$ or the subsequent $G_1$ phase, where they were then cryopreserved according to respective cell cycle phase (see Fig. 1).

For the γ-irradiation experiments, non-labeled synchronized cells were cryopreserved in S, $G_2/M$ or $G_1$ phase and irradiated. To achieve similar exposure conditions, cells were kept on dry ice and
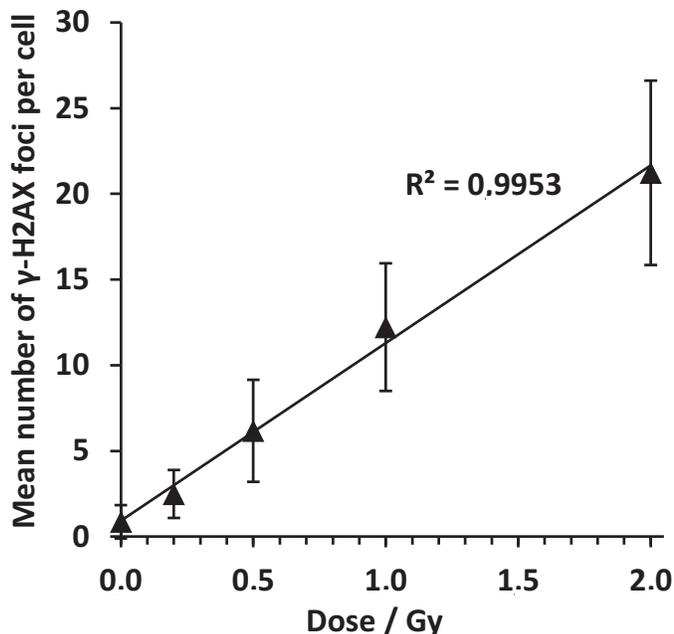
**FIG. 2.** Mean number of γ-H2AX foci per cell in asynchronous non-cryopreserved cells 45 min after γ-irradiation.

irradiated in the cryopreserved state using a $^{137}$Cs γ-ray source (Gammacell 40, Atomic Energy of Canada Limited, Mississauga, Canada) as previously described (*31*).

To monitor the cell cycle status, including during the synchronization and labeling steps as well as shortly before the cryopreservation of cells, small aliquots of $1.5 \times 10^5$ cells were taken from the suspended cell cultures. Aliquots were then centrifuged and after careful removal of the supernatant, the cell pellet was resuspended in DNA staining solution [0.05% Triton, 50 μl/ml 7-amino actinomycin D (7AAD) in PBS] and incubated for 10 mins at room temperature prior to cell cycle analysis using flow cytometry (FACSCanto II, BD Bioscience) as previously described (*31*).

After exposure to $^{125}$I-UdR, tritiated thymidine or γ rays, cells were thawed in a 37°C water bath and quickly transferred to pre-warmed standard growth medium. Cells were then centrifuged (5 min at 300 × g at RT) and after removing the supernatant, resuspended and cultured in standard growth medium ($1 \times 10^6$ cells per ml). All experiments were replicated at least three times. The γ irradiation of non-cryopreserved, asynchronous proliferating cells (Fig. 2) was carried out as previously reported (*31*).

### γ-H2AX Immunocytochemistry and Fluorescence Microscopy

After exposure in the cryopreserved state, cells were thawed in a water bath, quickly transferred to pre-warmed standard growth medium, centrifuged (5 min at 300 × g at RT) and, after removing the supernatant, resuspended and cultured in standard growth medium. The cells were then collected at different time points (0.5 h, 1 h, 2 h), centrifuged and washed twice with cold PBS (PAA Laboratories, Pasching, Austria). Prior to paraformaldehyde (PFA) fixation, cells were prepared on ice and centrifuged at 4°C. The PFA fixation and γ-H2AX-staining of Jurkat cells were performed as described previously (*31*) except that Alexa Fluor 594 goat anti-mouse IgG (H+L) (Life Technologies Corp., Eugene, USA) was used as the secondary antibody for γ-H2AX-staining. Anti-phospho-histone H2AX (139) clone JBW301 mouse antibody (1:700; Cat. no. 05-636; Merck, Darmstadt, Germany) was used as the primary antibody. As previously described (*31*), the stained cells were cytospinned and mounted with ProLong Gold Antifade Mounting Medium with DAPI (Invitrogen, Karlsruhe, Germany) and covered with 0.145 ± 0.015mm thick coverslips (22 × 40 mm; Menzel, Braunschweig, Germany). γ-H2AX foci

were evaluated and visually counted using an Axio Observer.Z1 fluorescence microscope [Zeiss (LSM 700), Göttingen, Germany]. Visual foci counting was performed by an experienced scorer, and the criteria for a focus was a diameter of approximately 0.5 μm and a brightness easily visible and consistent in controls and irradiated samples. Very small and faint signals were excluded. Well-defined γ-H2AX foci were counted as a single focus even if they slightly touched other foci. When evaluating the foci, the scorer focused through the entire cell nucleus. Fluorescence images of γ-H2AX-stained cells were taken on the Axio Observer.Z1 using immersion oil with a Zeiss Plan-APOCHROMAT 63×/1.4 oil DTC objective and using the integrated AxioCam. A total of at least 300 cells were counted for each data point. γ-H2AX-staining of asynchronous non-cryopreserved cells (Fig. 2) was carried out as described previously (*31*).

### Preparation and Quantification of CA

The same batches of exposed cells analyzed for γ-H2AX induction were used for CA analysis. However, after exposure in the cryopreserved state, Jurkat cells were thawed and cultured with 0.05 μg/ml colcemid (PAA Laboratories) for 24 h. Preparation was then performed according to the standard cytogenetic procedure established in our laboratory and described previously (*32*). After fixation with 3:1 methanol:acetic acid solution (Merck, Darmstadt, Germany), cells were dropped onto slides, air dried, and subsequently mounted with Vectashield Mounting Medium with 4¨,6-diamidino-2-phenylindole (DAPI) (Vector Laboratories, Burlingame, CA) and covered with coverslips (22 × 40 mm; Menzel). All types of aberrations (breaks, gaps, dicentrics, rings, triradial, quadrivalent) per metaphase were scored and added together to give the final aberration score. At least 300 metaphases were scored visually for each data point with a Zeiss Axioplan 2 fluorescence microscope.

To compare all radiation qualities and avoid microdosimetric approaches with rather high dose uncertainties especially for the low-energy Auger electrons, the average number of chromosomal aberrations was normalized to the average number of γ-H2AX foci for each radiation quality and cell cycle phase. Here, for γ-H2AX and CA data, controls were subtracted from the corresponding exposed samples, which thus represents solely the radiation-induced effect for both end points. For γ-H2AX, the maximum number of radiation-induced foci was used for each radiation quality and cell cycle phase to calculate the corresponding radiation-induced CA per radiation-induced γ-H2AX focus.

### RESULTS

Upon entry into S phase, synchronized Jurkat cells were pulse labeled with low activities of $^{125}$I-UdR or tritiated thymidine and either cryopreserved in S phase or further allowed to progress to G$_2$/M or G$_1$ phase, and then cryopreserved for days or weeks for decay/dose accumulation (approximately 50 $^{125}$I or 2,100 $^3$H decays/cell). Accordingly, Jurkat cells in the cryopreserved state were γ irradiated. The cell cycle-synchronization and exposure scheme is shown schematically in Fig. 1.

Cell cycle synchronization was highly efficient in all experiments and approximately 78 ± 3%, 75 ± 7% and 85 ± 2% entered the S, G$_2$/M and G$_1$ cell cycle phases synchronously, respectively. After thawing, cells were prepared to analyze the induction of γ-H2AX-foci and CA. However, to estimate an effect of cryopreservation on the induction of γ-H2AX foci, non-cryopreserved Jurkat cells were irradiated with γ rays. The γ-H2AX foci induction of γ-irradiated non-cryopreserved and proliferating Jurkat cells was shown to be almost linear ($R^2 = 0.9953$) as a function of dose (Fig. 2).
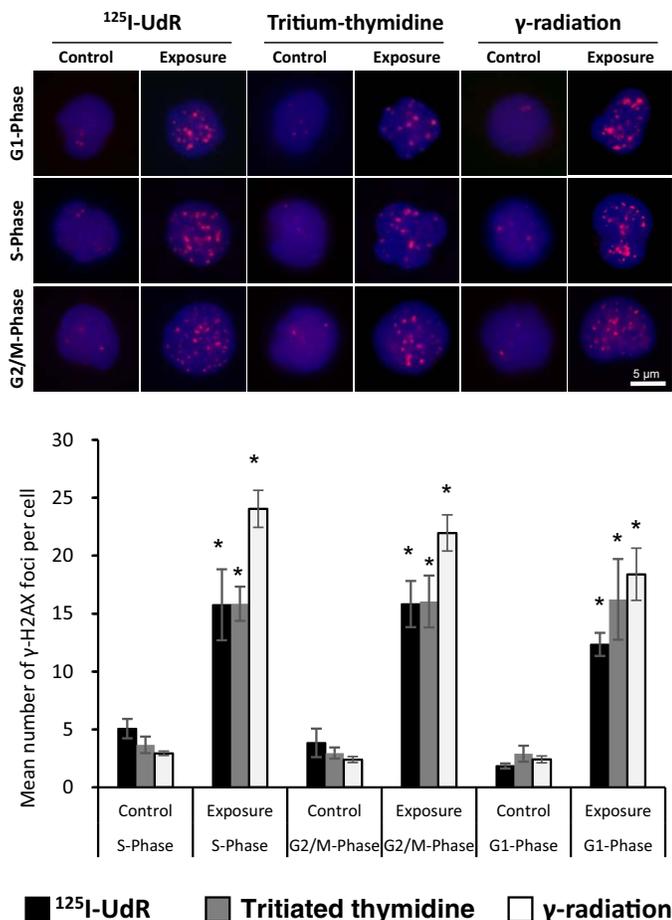
**FIG. 3.** Formation of γ-H2AX foci in Jurkat cells after exposure to [125]I (50 decays/cell), [3]H (2,100 decays/cell), or γ rays (10 Gy), respectively. γ-H2AX induction as mean number of foci per cell showed a significant increase compared to the respective controls (data tagged with *P < 0.05, Student's t-test).

After 1 and 2 Gy, 12.2 ± 3.7 and 21.2 ± 5.4 foci per cell were scored, respectively.

The cells exposed to ^{125}I-UdR, tritiated thymidine and [137]Cs γ rays in the cryopreserved state showed a significant increase of γ-H2AX foci per cell compared to the respective controls (Fig. 3). On average, 0.29 and 0.0076 foci per decay were induced by ^{125}I-UdR and tritiated thymidine, respectively. Hence, ^{125}I-UdR was approximately 38-times more effective per disintegration when compared to tritiated thymidine. A dose of 10 Gy γ radiation to cryopreserved Jurkat cells induced an average of 21.5 ± 2.3 foci per cell, which corresponded to 2 Gy (21.2 foci per cell) in γ-irradiated non-cryopreserved Jurkat cells.

The same batches of exposed cells analyzed for γ-H2AX induction were used for CA analysis. As shown in Fig. 4, the induction of CA per 100 metaphases was significantly increased for all radiation qualities compared to the respective controls. Approximately 255, 191, and 112 ^{125}I-UdR decays/disintegrations after exposure in $G_1$, S, and $G_2$/M phase, respectively, are necessary to induce on average one chromosomal aberration, while for tritiated thymidine, it
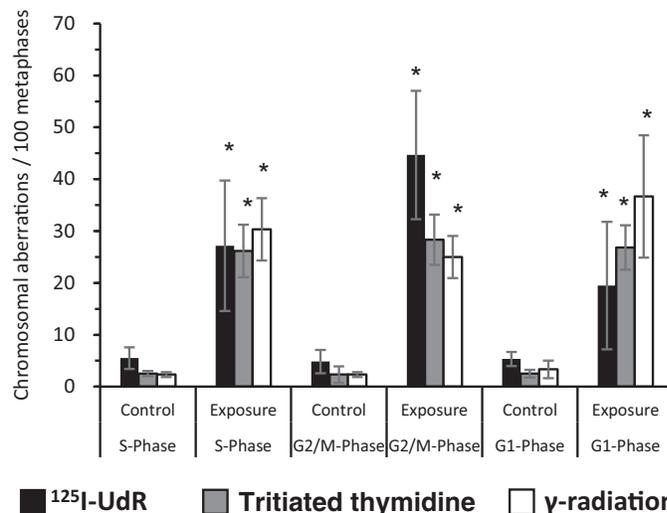


**FIG. 4.** The induction of chromosomal aberrations per 100 metaphases after exposure to ^{125}I-UdR (50 decays/cell), tritiated thymidine (2,100 decays/cell), and γ rays (10 Gy), respectively showed a significant increase compared to the respective controls (data tagged with *P < 0.05, Student's t-test).

took an average of 7,774 decays in the respective cell cycle phases.

To compare all radiation qualities and to avoid microdosimetry approaches with rather high dose uncertainties for the low-energy electron emitters, especially in the case of the AEE ^{125}I, the induction of chromosomal aberrations was normalized to the γ-H2AX foci per cell induction as a surrogate of induced DSB (Fig. 5). Exposure of S- or $G_1$-phase cells to ^{125}I-UdR, tritiated thymidine or [137]Cs γ rays did not result in any significant differences between the investigated radiation qualities regarding the induction of CA per γ-H2AX-foci/DSB. However, ^{125}I-UdR exposure of $G_2$/M cells resulted in a 2.9-fold increase (P = 0.018) of CA when compared to [137]Cs γ rays, and a 1.7-fold increase (P = 0.026) when compared to tritium exposure, respectively.
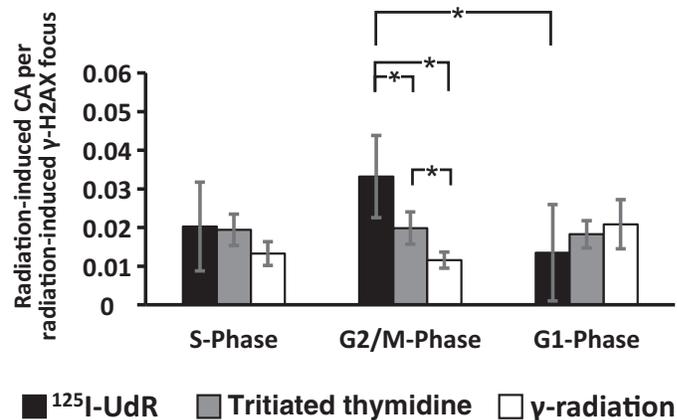


**FIG. 5.** Radiation-induced chromosome aberrations per radiation-induced γ-H2AX focus after exposure in the respective cell cycle phases. Data pairs marked with * were considered significant (P < 0.05, Student's t-test).

$G_2$/M cells exposed to $^3$H showed a smaller but still significant 1.7-fold increase (P = 0.025) of CA when compared to $G_2$/M cells exposed to $^{137}$Cs γ rays. In addition, $^{125}$I exposure of $G_2$/M cells showed a 2.5-fold increase (P = 0.023) of CA when compared to $G_1$-phase cells exposed to $^{125}$I.

Accordingly, based on the induced DSB measured by the γ-H2AX assay and assuming that one detected focus equals one DSB, it can be determined from Fig. 5 that 1 DSB induced by $^{125}$I-UdR, tritiated thymidine or $^{137}$Cs γ rays, respectively, lead to 0.033, 0.02 or 0.012 CA in $G_2$/M cells. Therefore, in $G_2$/M cells, $^{125}$I-UdR induced almost 3× and 1.7× more CA per DSB when compared to $^{137}$Cs γ rays and tritiated thymidine, respectively, whereas tritiated thymidine induced 1.7-times more CA per DSB when compared to $^{137}$Cs γ rays.

## DISCUSSION

In this study, the induction of CA was analyzed based on induced γ-H2AX foci as a surrogate of DSB induction. To question whether the complexity of DSB influences the overall formation of CA, we used three different radiation qualities, namely $^{125}$I, $^3$H and $^{137}$Cs γ rays (662 keV). $^{125}$I-UdR incorporated into DNA induces rather complex DNA damage and DSB (14, 15). This DNA damage causes similar effects to those induced by high-LET radiation, as indicated by similar cell survival curves lacking a shoulder region (16–18). Tritium incorporated into DNA shows a higher relative biological effectiveness compared to low-LET radiation such as gamma rays (19), and this is attributed to the low-energy β⁻ particle ejected during tritium decay.

γ-H2AX foci are widely regarded and accepted as a representation of DSB induction (27–30). In this study, an average of 0.29 γ-H2AX foci were induced per $^{125}$I decay from $^{125}$I-UdR incorporated into DNA. Yasui (33) determined 0.26 γ-H2AX foci per decay after exposure to $^{125}$I-UdR, which is in good agreement with our data. Yasui suspected that the number of γ-H2AX foci per $^{125}$I decay was underestimated because the cells were cryopreserved with 10% of the radical scavenger DMSO, as in the present work. DMSO is a potent radical scavenger and thus the mere number but also the diffusion of radiation-induced radicals is significantly reduced and result in a pronounced diminished extent of overall DNA damage. In contrast, Sedelnikova et al. (34), who exposed cells to $^{125}$I from incorporated $^{125}$I-UdR without cryopreservation, determined a rate of 0.8 γ-H2AX foci per $^{125}$I decay. The DMSO-associated pronounced reduction of DNA damage from cryopreservation seems also to be the explanation why, in our study, only 21.5 γ-H2AX foci/cell were induced in 10 Gy γ-irradiated cryopreserved Jurkat cells, which corresponded to the γ-H2AX induction detected in 2 Gy irradiated non-cryopreserved Jurkat cells. Zwicker et al. (35) showed a 1.6-fold reduction in γ-H2AX foci induction 30 min after 1 Gy irradiation in the presence of 2% DMSO and Kashino et al. (36) revealed a 3.3-fold reduction in 53BP1 foci induction 15 min after 0.2 Gy irradiation

in the presence of 5% DMSO. However, the cells in both studies were treated with DMSO without cryopreservation, in contrast to our study. Our observation that the reduction of foci induction was even more pronounced may be due to incubation with 10% DMSO and/or to the cryopreserved state of irradiated cells and thus the effective immobilization of radiation-induced reactive oxygen species (ROS). Indications that the presumed immobilization of ROS associated with cryopreservation additionally reduces the radiation effects were shown in DMSO-treated cells, which required a higher dose in the cryopreserved state than in the non-cryopreserved state to achieve the same radiation-induced effects with regard to CA (37) or cell survival (37, 38).

Non-cryopreserved Jurkat cells showed a linear dose-dependent increase with 12.2 foci induced after 1 Gy, which is consistent with the data of Leatherbarrow et al. (39) who showed 12.2 and 13.5 γ-H2AX foci/cell/Gy in V79-4 and XRS-5 cells under similar exposure conditions.

For tritiated thymidine, 0.0076 γ-H2AX foci per tritium decay were induced in our study. This is in very good agreement with foci induction rates of 0.007 and 0.008 γ-H2AX foci/decay derived from data of Saintigny et al. (40) determined in CHO-DRA10 and SMRAD51 cells after incorporation of tritiated thymidine. Thus, γ-H2AX foci, as a surrogate for DSB, induced by $^{125}$I-UdR, is about 38-times more effective per disintegration than tritiated thymidine. The mere number of ejected Auger electrons per decay might well explain why $^{125}$I is so much more effective in inducing DNA damage than tritium, which emits a single β⁻ particle during decay with an average energy of 5.7 keV. In general, AEE eject a shower of low-energy electrons during decay; in the case of $^{125}$I, an average of 13 Auger electrons are ejected (13). Due to their very low energy, most Auger electrons have a very short range of only 1–10 nm (9). When located within the DNA double helix, the vast majority of the released energy is, therefore, deposited in the DNA molecule in the close vicinity of the decaying AEE, leading to clustered ionizations. In contrast, beta emitters such as tritium emit a single electron with a much longer range (about 0.56 μm in case of tritium), which rarely leads to clustered ionizations (41).

Iodine-125 showed 31- to 67-times higher efficiency per decay (depending on cell cycle position) than tritium with respect to CA and γ-H2AX foci induction. While tritiated thymidine required an average of 7,774 decays, $^{125}$I-UdR required only 112 to 255 decays (depending on cell cycle position) to induce one chromosomal aberration. Similar to our results, Schmitz et al. (32) showed in lymphocytes that 250 decays were required to induce one chromosomal aberration after exposure to $^{125}$I-UdR. Chan et al. (42) exposed V79 Chinese hamster cells to $^{125}$I-UdR or tritiated thymidine without cryopreservation and showed that 0.1 pCi $^{125}$I per cell resulted in three chromosome breaks per cell, while a 17-fold activity of $^3$H (1.7 pCi per cell) was required to achieve the same effect, which is in accordance with our results regarding the effectiveness of $^{125}$I-UdR. Calculating

the accumulated decays from the data of Chan et al. (42), 71 $^{125}$I and 1,208 $^3$H decays per cell, respectively, are required to produce one chromosomal aberration, whereas in our study, approximately 112 to 255 $^{125}$I or 7,774 $^3$H decays are required. But, again, this discrepancy is probably because the cells in our study were cryopreserved in the presence of DMSO, which significantly reduced DNA damage induction, as discussed above. Interestingly, the cryopreservation procedure with DMSO appears to have a much larger effect on reducing initial DNA damage in case of tritiated thymidine than $^{125}$I-UdR. This may be due to the fact that $^{125}$I-UdR deposits much of the dose via direct interactions to the DNA rather than by indirect effects via ROS-mediated interactions, as already indicated by computer simulations of Terrissol et al. (43). Therefore, our experimental data verified and validated for the first time the computer simulations of Terrissol et al. (43).

Our study showed that $^{125}$I-UdR, tritiated thymidine and $^{137}$Cs γ rays significantly induced CA at all cell cycle stages. To compare the different radiation qualities, the CA were normalized to the γ-H2AX foci or initial DSB induction, similar to a study using comet assay data (18). While no differences were found between the three radiation qualities with respect to exposure in the S or $G_1$ phase, exposure in the $G_2$/M phase showed an approximately threefold greater radiosensitivity with respect to conversion of DSB to CA after $^{125}$I exposure, when compared to low-LET γ radiation, but also when compared to $^{125}$I exposure in the $G_1$ phase. That $^{125}$I-UdR is more likely to induce chromosomal aberrations in $G_2$/M cells than in $G_1$ cells per disintegration might be attributed, at first glance, to the fact that the cells in $G_2$/M are the most radiosensitive, while cells in $G_1$ phase show intermediate overall radiosensitivity when external irradiation is considered (21). However, the question arises why $^{125}$I exposure in $G_2$/M in particular, leads to increased induction of CA per decay. One reason could be the induction of highly complex DNA lesions by $^{125}$I. Complex DNA lesions are predicted for DNA-associated AEE like $^{125}$I-UdR (14, 15). This is highly plausible since the emission of many short-range Auger electrons deposit large amounts of energy in a very small volume in close vicinity to the decay site and is, thus, similar to high-LET radiation in terms of its radiobiological effectiveness (10–12). Additionally, $^{125}$I-UdR incorporation induces a high-LET type DNA damage pattern with respect to SSB/DSB ratio as comet assay analyses (18) and computer simulations showed (44). Moreover, $^{125}$I-UdR and $^{125}$I-labeled DNA-binding triplex-forming-oligonucleotides (TFO) cause high-LET type biological effects e.g., exponential cell killing using a colony-forming assay (16, 17, 45), which is again very likely due to the complexity of the induced DNA lesions. As with high-LET particle radiation (6–8), these complex DNA lesions might cause DSB repair to be more often incomplete and, therefore, are more likely to lead to CA.

In addition to $^{125}$I, $^3$H-exposed $G_2$/M cells also showed a 1.7-fold increased induction of CA per induced γ-H2AX focus compared to γ-irradiated $G_2$/M cells, albeit to a lesser extent than $^{125}$I. UNSCEAR gives a mean RBE of 1.5-2 for $^3$H, based on in vitro and in vivo experiments and using γ rays as a reference radiation source (19). It is very likely that the complexity of the DNA damage contributes to the results found in our study for tritiated thymidine. Using computer simulations, Moiseenko et al. (46) showed that $^3$H induces complex DSB, defined as DSB with additional strand breaks, with a RBE of 1.3 compared to γ radiation. We want to highlight that $^{125}$I induces 1.7 times more CA per γ-H2AX foci than $^3$H in $G_2$/M cells, indicating that DNA-incorporated AEE induce DSB of a particularly high initial complexity, making them a promising candidate for targeted therapeutical applications in nuclear medicine and in DNA-repair research.

However, to discuss fully the results of this study, it is necessary to consider not only the initial complexity of the DNA lesions, but also, the cell cycle-dependence of DNA/chromatin architecture, lesion induction, and repair. Chromatin is relaxed and open in the S phase, where DNA replication takes place, as well as in the transcriptionally active $G_1$ phase, with the exception of the heterochromatic regions. In contrast, chromatin is more condensed and/or already densely packed in $G_2$ phase and, of course, maximally condensed in mitosis (21). When DNA damage is induced by radiation, the chromatin structure at the sites of DNA damage is opened, making the DNA damage more accessible to repair enzymes (21). Such a radiation-induced chromosome conformational state is thought to be biologically and thermodynamically unfavorable and, hence, unstable for the folding or unfolding of conformational changes of chromosomes during the cell cycle (21). If chromosome conformation changes shortly after irradiation, depending on the stage of the cell cycle, these chromatin dynamics could lead to mechanical stress and breakage of unfolded chromatin at the sites of DNA lesions during their repair, resulting in CA (21).

DNA lesions induced by $^{125}$I-UdR are complex, but might still vary in the degree of complexity of the DNA damage pattern depending on how densely packed the DNA/chromatin architecture is. It would be conceivable that lesions induced by $^{125}$I-UdR in more densely packed $G_2$/M phase chromatin would be even more complex, difficult to repair and more likely to lead to CA when compared to lesions induced in decondensed and more relaxed $G_1$ phase chromatin. It would additionally explain why, of all three investigated radiation qualities in this study, $^{125}$I-UdR is effective in inducing CA when exposure takes place in $G_2$/M phase.

The data in our study indicate that the 3D organization of replicated DNA/chromatin in $G_2$/M seems to be prone to more complex DNA lesions when compared to the DNA/chromatin architecture in S or $G_1$ cells. Whether this is due to DNA organization itself or to DNA repair inefficiency should be further investigated.

## REFERENCES

1. Burkart W, Jung T, Frasch G. Damage pattern as a function of radiation quality and other factors. Cr Acad Sci Iii-Vie 1999; 322(2-3):89-101.

2. Jenner TJ, Delara CM, Oneill P, Stevens DL. Induction and rejoining of DNA double-strand breaks in V79-4 mammalian-cells following gamma-irradiation and alpha-irradiation. Int J Radiat Biol 1993; 64(3):265-73.

3. Ottolenghi A, Merzagora M, Paretzke HG. DNA complex lesions induced by protons and alpha-particles: track structure characteristics determining linear energy transfer and particle type dependence. Radiat Environ Biophys 1997; 36(2):97-103.

4. Prise KM, Folkard M, Newman HC, Michael BD. Effect of radiation quality on lesion complexity in cellular DNA. Int J Radiat Biol 1994; 66(5):537-42.

5. Karlsson KH, Stenerlow B. Focus formation of DNA repair proteins in normal and repair-deficient cells irradiated with high-LET ions. Radiat Res 2004; 161(5):517-27.

6. Takahashi A, Yamakawa N, Kirita T, Omori K, Ishioka N, Furusawa Y, et al. DNA Damage Recognition Proteins Localize along Heavy Ion Induced Tracks in the Cell Nucleus. J Radiat Res 2008; 49(6):645-52.

7. Stenerlow B, Hoglund E, Carlsson J, Blomquist E. Rejoining of DNA fragments produced by radiations of different linear energy transfer. Int J Radiat Biol 2000; 76(4):549-57.

8. Ritter S, Durante M. Heavy-ion induced chromosomal aberrations: A review. Mutat Res-Genet Toxicol Environ Mutag 2010; 701(1):38-46.

9. Howell RW. Auger processes in the 21st century. Int J Radiat Biol. 2008; 84(12):959-75.

10. Balagurumoorthy P, Chen K, Adelstein SJ, Kassis AI. Auger electron-induced double-strand breaks depend on DNA topology. Radiat Res 2008; 170(1):70-82.

11. Kassis AI, Adelstein SJ. Radiobiologic principles in radionuclide therapy. J Nuc Med 2005; 46 Suppl 1:4S-12S.

12. Boyd M, Sorensen A, McCluskey AG, Mairs RJ. Radiation quality-dependent bystander effects elicited by targeted radionuclides. J Pharm Pharmacol 2008; 60(8):951-8.

13. Pomplun E. Monte Carlo simulation of Auger electron cascades versus experimental data. Biomed Phys Eng Express 2016; 2(1): 015014.

14. Pomplun E, Terrissol M, Hille R. Ratio of Complex Double Strand Break Damage Induced by 125IUdR and 123IUdR Correlates with Experimental In Vitro Cell Killing Effectiveness. Radiat Prot Dosimet 2002; 99(1-4):81-2.

15. Kassis A, Sastry K, Adelstein S. Kinetics of uptake, retention, and radiotoxicity of 125IUdR in mammalian cells: implications of localized energy deposition by Auger processes. Radiat Res 1987; 109(1):78-89.

16. Howell RW, Rao DV, Hou DY, Narra VR, Sastry KS. The question of relative biological effectiveness and quality factor for auger emitters incorporated into proliferating mammalian cells. Radiat Res 1991; 128(3):282-92.

17. Rao DV, Narra VR, Howell RW, Govelitz GF, Sastry KS. In-vivo radiotoxicity of DNA-incorporated 125I compared with that of densely ionising alpha-particles. Lancet 1989; 2(8664):650-3.

18. Unverricht-Yeboah M, Holtmann K, Kriehuber R. Comet Assay analysis of DNA strand breaks after exposure to the DNA-incorporated Auger Electron Emitter Iodine-125. Int J Radiat Biol 2023; 99(1): 64-9.

19. United Nations Scientific Committee on the Effects of Atomic Radiation Report to the General Assembly. Scientific Annexes A B, C, D. UNSCEAR 2016 Report—Sources, Effects and Risks of Ionizing Radiation. 2017.

20. Terrissol M, Peudon A, Kummerle E, Pomplun E. On the biological efficiency of I-123 and I-125 decay on the molecular level. Int J Radiat Biol 2008; 84(12):1063-8.

21. Terzoudi GI, Hatzi VI, Donta-Bakoyianni C, Pantelias GE. Chromatin dynamics during cell cycle mediate conversion of DNA damage into chromatid breaks and affect formation of chromosomal aberrations: biological and clinical significance. Mutat Res 2011; 711(1-2):174-86.

22. Mahaney Brandi L, Meek K, Lees-Miller Susan P. Repair of ionizing radiation-induced DNA double-strand breaks by non-homologous end-joining. Biochem J 2009; 417(3):639-50.

23. Chang HHY, Pannunzio NR, Adachi N, Lieber MR. Non-homologous DNA end joining and alternative pathways to double-strand break repair. Nat Rev Mol Cell Biol 2017; 18(8):495-506.

24. Wright WD, Shah SS, Heyer W-D. Homologous recombination and the repair of DNA double-strand breaks. J Biol Chem. 2018; 293(27):10524-35.

25. Shibata A, Conrad S, Birraux J, Geuting V, Barton O, Ismail A, et al. Factors determining DNA double-strand break repair pathway choice in G2 phase. EMBO J 2011; 30(6):1079-92.

26. Rucinski A, Biernacka A, Schulte R. Applications of nanodosimetry in particle therapy planning and beyond. Phys Med Biol 2021; 66(24):24TR01.

27. Rothkamm K, Horn S. Gamma-H2AX as protein biomarker for radiation exposure. Ann Ist Super Sanita 2009; 45(3):265-71.

28. Gerić M, Gajski G, Garaj-Vrhovac V. γ-H2AX as a biomarker for DNA double-strand breaks in ecotoxicology. Ecotoxicol Environ Saf 2014; 105:13-21.

29. Kuo LJ, Yang LX. Gamma-H2AX - a novel biomarker for DNA double-strand breaks. In Vivo 2008; 22(3):305-9.

30. Sharma A, Singh K, Almasan A. Histone H2AX phosphorylation: a marker for DNA damage. Methods Mol Biol 2012; 920:613-26.

31. Unverricht-Yeboah M, Giesen U, Kriehuber R. Comparative gene expression analysis after exposure to 123I-iododeoxyuridine, γ- and α-radiation-potential biomarkers for the discrimination of radiation qualities. J Radiat Res 2018; 59(4):411-29.

32. Schmitz S, Oskamp D, Pomplun E, Kriehuber R. Corrigendum to "Chromosome aberrations induced by the Auger electron emitter 125I" [Mut Res.—Genet. Toxicol. Environ. Mutagen. 793 (2015) 64–70]. Mut Res 2016; 800-801:46.

33. Yasui LS. GammaH2AX foci induced by gamma rays and 125idU decay. Int J Radiat Biol 2004; 80(11-12):895-903.

34. Sedelnikova OA, Rogakou EP, Panyutin IG, Bonner WM. Quantitative detection of (125)IdU-induced DNA double-strand breaks with gamma-H2AX antibody. Radiat Res 2002; 158(4):486-92.

35. Zwicker F, Hauswald H, Debus J, Huber PE, Weber KJ. Impact of dimethyl sulfoxide on irradiation-related DNA double-strand-break induction, -repair and cell survival. Radiat Envir Biophys 2019; 58(3):417-24.

36. Kashino G, Liu Y, Suzuki M, Masunaga S, Kinashi Y, Ono K, et al. An alternative mechanism for radioprotection by dimethyl sulfoxide; possible facilitation of DNA double-strand break repair. J Radiat Res 2010; 51(6):733-40.

37. Watanabe M, Suzuki M, Suzuki K, Hayakawa Y, Miyazaki T. Radioprotective effects of dimethyl sulfoxide in golden hamster embryo cells exposed to gamma rays at 77 K. II. Protection from lethal, chromosomal, and DNA damage. Radiat Res 1990; 124(1): 73-8.

38. Limoli CL, Kaplan MI, Giedzinski E, Morgan WF. Attenuation of radiation-induced genomic instability by free radical scavengers and cellular proliferation. Free Rad Biol Med 2001; 31(1): 10-9.

39. Leatherbarrow EL, Harper JV, Cucinotta FA, O'Neill P. Induction and quantification of gamma-H2AX foci following low and high LET-irradiation. Int J Radiat Biol 2006; 82(2):111-8.

40. Saintigny Y, Roche S, Meynard D, Lopez BS. Homologous recombination is involved in the repair response of mammalian cells to low doses of tritium. Radiat Res 2008; 170(2):172-83.

41. Siragusa M, Fredericia PM, Jensen M, Groesser T. Radiobiological effects of tritiated water short-term exposure on V79 clonogenic cell survival. Int J Radiat Biol 2018; 94(2):157-65.

42. Chan PC, Lisco E, Lisco H, Adelstein SJ. The radiotoxicity of iodine-125 in mammalian cells II. A comparative study on cell survival and cytogenetic responses to 125IUdR, 131TUdR, and 3HTdR. Radiat Res 1976; 67(2):332-43.

43. Terrissol M, Edel S, Pomplun E. Computer evaluation of direct and indirect damage induced by free and DNA-bound iodine-125 in the chromatin fibre. Int J Radiat Biol 2004; 80(11-12):905-8.

44. Pomplun E, Terrissol M, Demonchy M. Modelling of initial events and chemical behaviour of species induced in DNA units by Auger electrons from 125I, 123I and carbon. Acta Oncol 1996; 35(7):857-62.

45. Dahmen V, Pomplun E, Kriehuber R. Iodine-125-labeled DNA-Triplex-forming oligonucleotides reveal increased cyto- and genotoxic effectiveness compared to Phosphorus-32. Int J Radiat Biol 2016; 92(11):679-85.

46. Moiseenko VV, Waker AJ, Hamm RN, Prestwich WV. Calculation of radiation-induced DNA damage from photons and tritium beta-particles. Part II: Tritium RBE and damage complexity. Radiat Environ Biophysics 2001; 40(1):33-8.